ELSEVIER

Image and Vision Computing 16 (1998) 689–701

image AND vision COMPUTING

The Fourier slice theorem for range data reconstruction

Chiou-Shann Fuh*, Shih-Schön Lin

Department of Computer Science and Information Engineering, National Taiwan University, Taipei, Taiwan, ROC

Received 10 February 1997; accepted 13 October 1997

Abstract

This paper proposes a new approach to resolve the ambiguity problem in multistriping laser triangulation systems [1]. The application of this new method to circularly symmetrical objects can achieve time and space complexity of order one. No optical shutter is required in this new method.

The new solution is based on the Fourier slice theorem, which forms the basis of X-ray CT (computed tomography) reconstruction. This paper demonstrates how this theorem can also be used to resolve multistripe laser ambiguity effectively.

Keywords: Multistripe laser triangulation; Fourier slice theorem; 3-D data reconstruction; Structured lighting; Range image

1. Introduction

In order to recover the third dimension from 2-D pictures, one series of techniques devised by the precursors in this field is as follows:

- structured lighting to resolve the line of sight [2];
- multistriped laser pattern to increase the scanning area [3];
- optical shutter pattern to resolve ambiguity of the multistriped laser pattern [4].

Several other methods have also been proposed by ingenious workers in this field [5,6]. Each method employs different heuristics and laws of physics, and no single method could outperform all other methods in every situation. Interested readers can find a general survey in [7]. The principle of structured light ranging systems is triangulation; see Fig. 1(a). Stereo pair ranging also uses triangulation, but it is difficult to match corresponding points out of the stereo image pairs. The structured light method, on the other hand, can easily pinpoint the position of a distinctive light stripe (Fig. 2) and resolve the depth [8]. However, as we increase the number of stripes we see in one image, another ambiguity problem arises. We will discuss this problem in greater detail in the next section, as this is the major problem we are going to solve.

The Fourier slice theorem is the backbone of X-ray computed tomography (CT) [9]. This theorem states that if the projection function (Radon transform) of a 2-D surface $f(x, y)$ is known at every angle, one can uniquely recover the individual value $f(a, b)$ for any point (a, b). For incomplete angular range reconstruction, see [10]. We would show that the problem we discuss can be reduced to the recovery of a conceptual $f(x, y)$, and we devise a new approach to solving our problem by means of the Fourier slice theorem.

2. The multistripe laser ambiguity problem and optical shutter solution

2.1. The ambiguity problem

Suppose we are inspecting industrial parts on a conveyor belt. Before the parts are fed in, the camera sees approximately equally spaced laser stripes on the flat conveyor belt. We call the image positions of each stripe the starting positions of the stripes when there are no objects on the conveyor belt. Once the objects of interest come into the inspection area, our camera would see the positions of the laser stripes move. We call the image positions after the objects of interest have entered the inspection area the ending positions of each stripe. Such displacements in our 2-D raw data are related to the 3-D depth information we want.

To calculate displacements we need both the starting positions and the ending positions. Unfortunately, raw data give only the ending positions. When we use only one laser stripe, we get displacements easily because we control one and only one stripe, so we know where each

* Corresponding author. E-mail: r3506011@image.csie.ntu.edu.tw, fuh@csie.ntu.edu.tw

0262-8856/98/$19.00
PII S0262-8856(98)00081-X

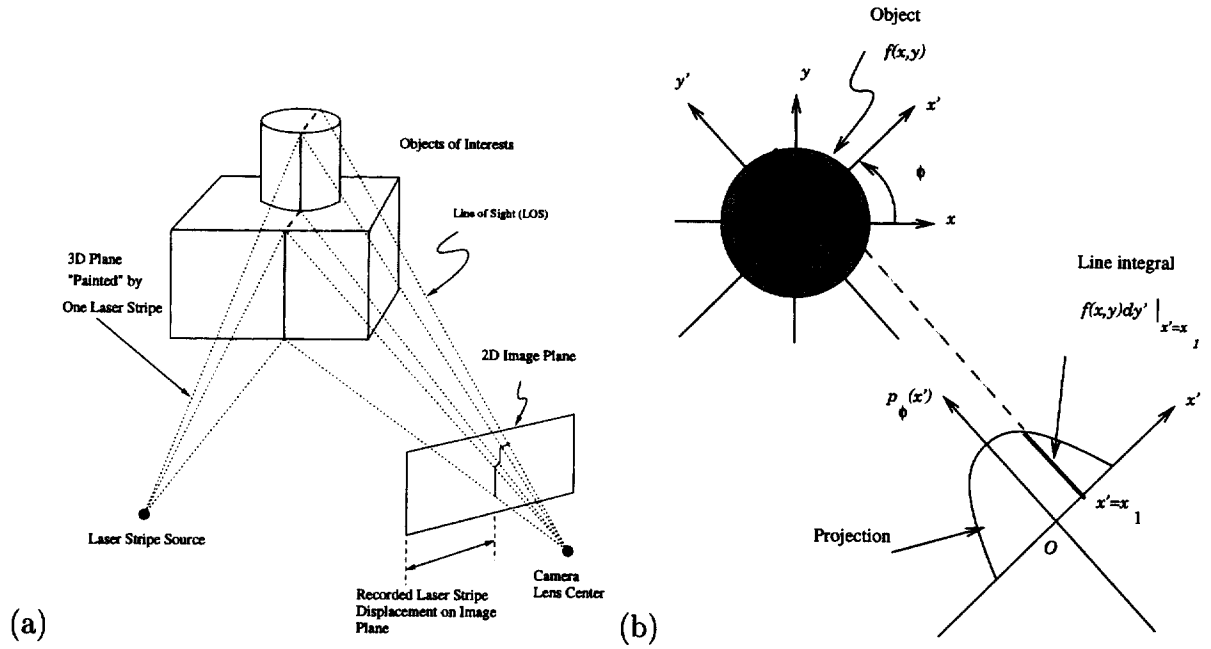

Fig. 1. (a) The role of the laser in triangulation: by projecting one laser stripe (lighting with known structure, i.e. structured light), we resolve the line-of-sight ambiguity. Prior to the projection of the laser stripe, we only know that one real-world point on the line of sight is imaged. After the projection of the laser stripe, we know exactly which world point is imaged, i.e. the point of intersection between the laser stripe plane and the line of sight of the corresponding image point. (b) Radon transform or projection data of 2-D surface function $f(x, y)$ at a given view angle ϕ.

starting position is before the object comes into sight. Once we project more than one stripe at the same time, we lose track of which starting point corresponds to which ending point. This is the so-called multistriping ambiguity problem. Note that we still know all the values of the starting and ending positions in multistriping systems; we lose only their correspondences. This is the key element of our method to recover the lost information.

2.2. Optical shutter solution

A mechanical or electrical solution to the multistriping ambiguity problem is to add optical shutters in front of each of the stripes we project. Optical shutters allow more control over the light stripes. By turning on one stripe at a time, the ambiguity disappears. This time we do not have to scan the stripe or move the object, which reduces the errors introduced in the scanning process. If we number the stripes and 'switch' on and off the bits of each number, then we can reduce the number of images taken in one 'scan' to the logarithm of the number of stripes provided; see [4].

2.3. Motivation for alternative solutions

Unfortunately, one may not always have easy access to the specific control electronics and optical components for shuttering. Moreover, if we can do the job without adding mechanical or electronic gadgets, we save money and at the same time increase system reliability. Should the sophisticated controls needed by existing algorithms break down at crucial moments, those algorithms cease to function as well. Our proposed solution fills this gap.

3. Mathematical background

3.1. Perspective projection

Basically, each point in an image represents one line of sight (LOS); see Fig. 1(a). When the center of perspective projection is distant from the image plane, perspective projection can be approximated by orthogonal projection.

3.2. Radon transform

The Radon transform operator for a given function f (see Fig. 1(b)) is defined as

$$p_\phi(x') \equiv \mathcal{R}[f(x, y)]$$

$$= \int_{-\infty}^{\infty}\int f(x, y)\delta(x\cos\phi + y\sin\phi - x')\mathrm{d}x\mathrm{d}y$$

$$= \int_{-\infty}^{\infty} f(x'\cos\phi - y'\sin\phi,\ x'\sin\phi + y'\cos\phi)\mathrm{d}y'$$

where

$$\begin{bmatrix} x' \\ y' \end{bmatrix} = \begin{bmatrix} \cos\phi & \sin\phi \\ -\sin\phi & \cos\phi \end{bmatrix} \begin{bmatrix} x \\ y \end{bmatrix}$$

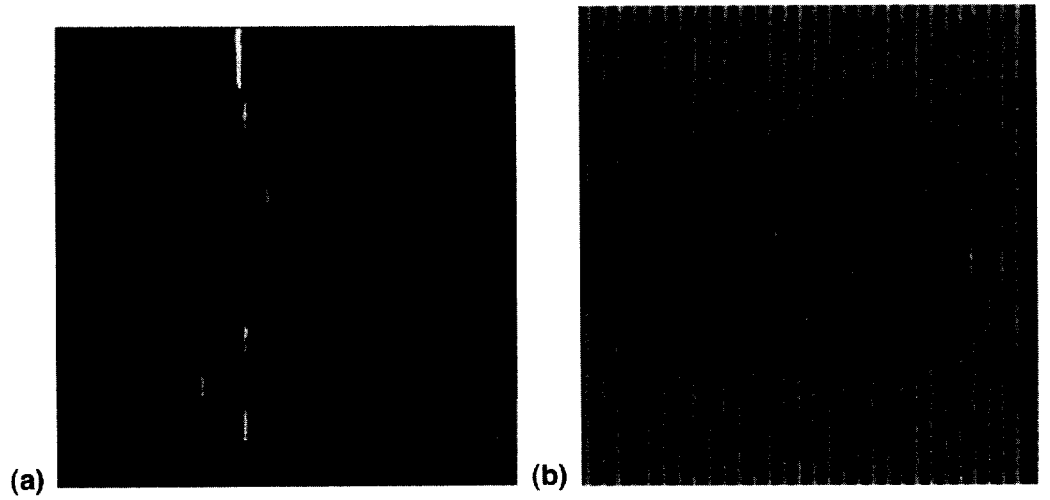

Fig. 2. (a) Actual image taken by single-stripe laser triangulation system. (b) Typical image of multi-stripe laser triangulation system.

3.3. Fourier transform

The 1-D Fourier transform of a function $f(x)$ is defined as

$$\mathcal{F}_1[f(x)] \equiv F(\omega_x) = \int_{-\infty}^{\infty} f(x) \exp\{-i(\omega_x x)\}\mathrm{d}x$$

The 2-D Fourier transform of an image function $f(x, y)$ is defined as

$$\mathcal{F}_2[f(x, y)] \equiv F(\omega_x, \omega_y) = \int_{-\infty}^{\infty}\int f(x, y) \exp\{-i(\omega_x x + \omega_y y)\}\mathrm{d}x\mathrm{d}y$$

4. The proposed new solution

4.1. Physical model

For illustration, let us consider the case that we project $2p+1$ stripes which form straight lines parallel to the y-axis of the image when there is nothing but the calibration board on our inspection table. Here we assume the camera is looking right on top of the inspection table, and orthogonal projection can be used to approximate perspective projection. Also, we assume the image taken can resolve $2n+1$ data points. For convenience of discussion and ease of implementation, we assume the undistorted laser stripes are seen as several columns of bright pixels or rows of bright pixels. This is easily achievable in our system; see Fig. 2(b). Then we can construct a conceptual discrete 2-D domain with x ranging from $-p$ to p and y ranging from $-n$ to n; see Fig. 3. We use the function $f(x, y)$ to calculate the 3-D depth:

$$f(x, y) = l_1(x, y) - l_0(x, y)$$

where $l_0(x, y)$ is the position of the xth laser stripe at the yth row on the image when there is no object on the inspection table, whereas $l_1(x, y)$ is the position of the xth laser stripe at the yth row on the image when there is an object on the inspection table. We know exactly the function value $l_0(x, y)$ for every (x, y) in our domain because the spatial ordering of laser stripes in the calibration image is under our control, but we usually cannot predict the ordering when the inspected objects come into play. In short, suppose we still get $2p+1$ stripes and their positions, we are still unsure which value belongs-to which $l_1(x, y)$.

Now let us take a look at the discrete Radon transform (see Fig. 1(b)) along the y-axis of our domain:

$$\begin{aligned} p_{(\pi/2)}(x') &\equiv \mathcal{R}[f(x, y)] \\ &= \sum_x \sum_y f(x, y)\delta(x\cos\tfrac{\pi}{2} + y\sin\tfrac{\pi}{2} - x')\Delta x\Delta y \\ &= \sum_{y'} f(-y', x')\Delta y' \\ &= \sum_{\xi} f(\xi, x')\Delta\xi \\ &= \sum_{\xi} \big(l_1(\xi, x') - l_0(\xi, x')\big)\Delta\xi \\ &= \sum_{\xi} l_1(\xi, x')\Delta\xi - \sum_{\xi} l_0(\xi, x')\Delta\xi \end{aligned}$$

Both the last two summations are calculable regardless of whether we can match the values to their respective $l_1(x, y)$ or not.

4.2. How the Radon and Fourier transforms come into play

Assume that the object surface to be inspected is sufficiently smooth so that we can approximate its Radon transform of our conceptual domain at many other angles

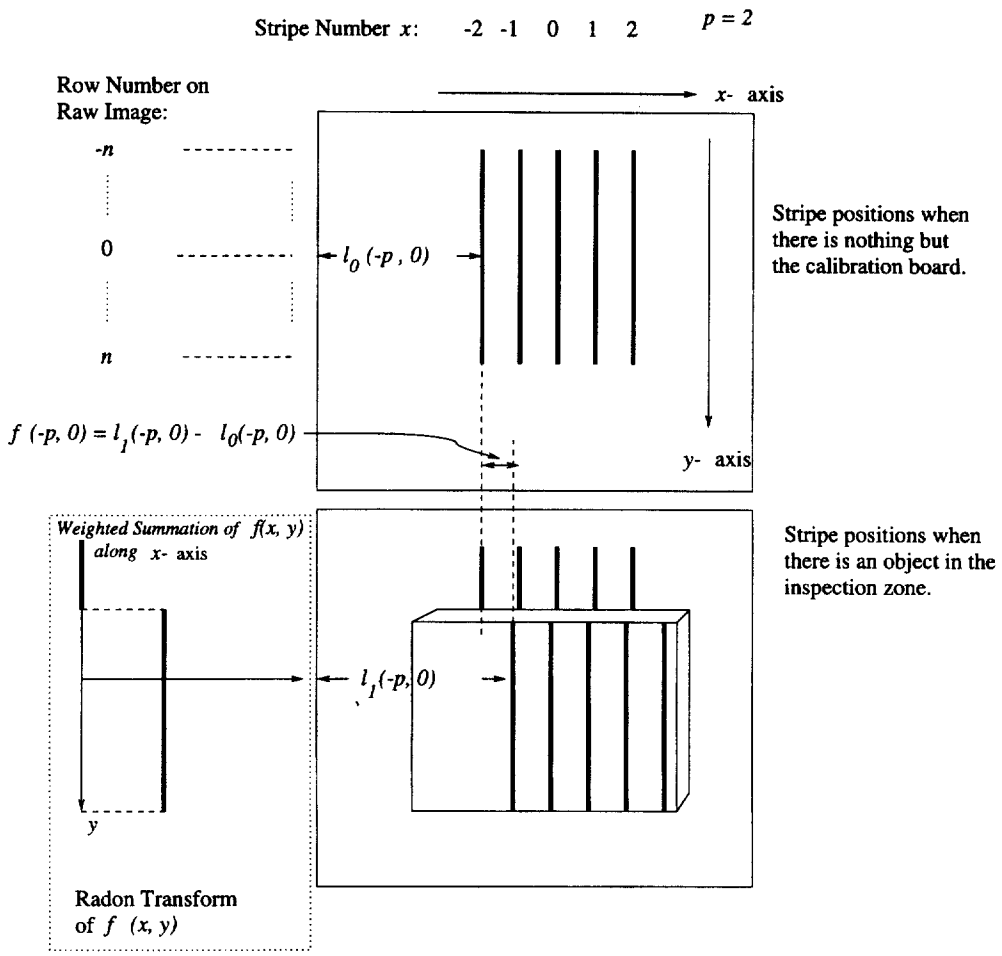

Fig. 3. The physical meaning of conceptual function $f(x, y)$.

by taking pictures as we change the relative angles between the inspection imaging system and the object. Then we can proceed with the application of the Fourier slice theorem (also called the projection theorem) to resolve $(2n + 1) \times (2p + 1)$ pairs of correspondences altogether.

Consider the 1-D Fourier transform of the Radon transform

$$P_\phi(\omega) \equiv \mathcal{F}_1[p_\phi(x')]$$

$$= \int_{-\infty}^{\infty} p_\phi(x') \exp(-i\omega x')\mathrm{d}x'$$

$$= \int \int_{-\infty}^{\infty} f(x' \cos\phi - y' \sin\phi,\ x' \sin\phi + y' \cos\phi)$$

$$\times \exp(-i\omega x')\mathrm{d}x'\mathrm{d}y'$$

$$= \int \int_{-\infty}^{\infty} f(x,\ y) \exp[-i\omega(x \cos\phi + y \sin\phi)]\mathrm{d}x\mathrm{d}y$$

$$= F(\omega \cos\phi,\ \omega \sin\phi)$$

$$= F(\omega_x,\ \omega_y)|_\phi$$

$$= F(\omega,\ \phi)$$

Note that $\mathcal{F}_1$ stands for the 1-D Fourier transform. The last form is the 2-D Fourier transform of the conceptual function $f(x, y)$ presented in the Fourier domain polar coordinates. This means that the 1-D Fourier transform of the projection data (Radon transform) at a given view angle is equivalent to the radial data passing through the origin at a given angle ϕ in the 2-D Fourier transform domain data.

So, if we get sufficient sampling in many view angles or we know in advance that the object possesses certain forms of symmetry, then we can in principle fill out the 2-D Fourier transform of our intended domain, and the inverse transform, to reconstruct our desired function.

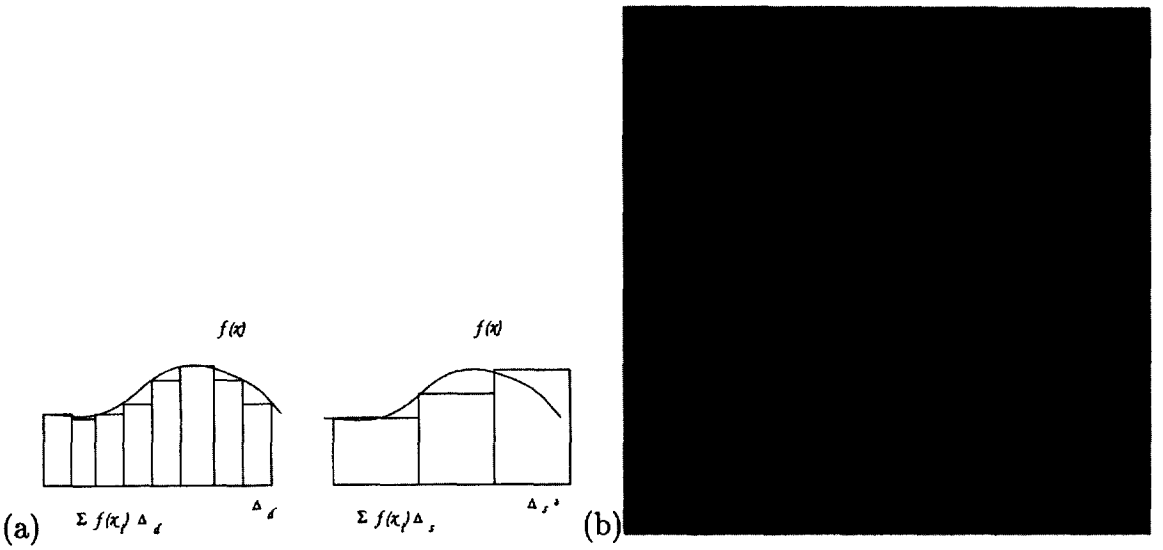

Fig. 4. (a) Densely sampled digital integration (left), and sparsely sampled digital integration (right). (b) Recovered range data for Fig. 2(b) (rms = 1.6 mm). The rings are caused by ringing effects. We used only one picture to reconstruct this range image (rms = root mean square error).

4.3. Implementation: the discrete Fourier transform and back projection

Actually, when it comes to real implementation, things are far more complicated than the ideal theorem stated above. So far, the theorem is derived purely from continuous domains, but all we get in a real-world application is sampled discrete data. So techniques such as the Filtered Backprojection (FB) and the Backprojection Filtering (BF) algorithms [9] were developed to handle these real-world imperfections.

Consider the inverse 2-D Fourier transform in frequency domain polar coordinates (ω, ϕ) and space domain polar coordinates (r, θ).

$$\hat{f}(r,\theta) = \int_0^{2\pi}\int_0^{\infty} F(\omega,\phi)\exp[i\omega(x\cos\phi + y\sin\phi)]|\omega|\mathrm{d}\omega\mathrm{d}\phi$$

$$= \int_0^{\pi}\int_{-\infty}^{\infty} |\omega| P_\phi(\omega)\exp[i\omega(x\cos\phi + y\sin\phi)]\mathrm{d}\omega\mathrm{d}\phi$$

$$= \int_0^{\pi} p_\phi^*(x')\mathrm{d}\phi$$

where

$$p_\phi^*(x') = \int_{-\infty}^{\infty} |\omega| P_\phi(\omega)\exp(i\omega x')\mathrm{d}\omega$$

$$= \mathcal{F}_1^{-1}[|\omega| P_\phi(\omega)]$$

$$= \mathcal{F}_1^{-1}[|\omega|] * p_\phi(x')$$

Note here that $\mathcal{F}^{-1}$ stands for the 1-D inverse Fourier transform. In actual implementation, we would use the discrete Fourier transform (DFT) to obtain $P_\phi(\omega)$ and the inverse discrete Fourier transform (iDFT) to obtain $p_\phi^*(x')$ [11]. Another approach is to derive $\mathcal{F}_1^{-1}[|\omega|]$ analytically and sample the results in the spatial domain. Note here that with either approach we get the values of $p_\phi^*(x')$ only for a fixed number of x's. However, when we evaluate $\hat{f}(r, \theta)$, we need for each ϕ the value of $p_\phi^*(x')$ at $x' = x\cos\phi + y\sin\phi$. In such a case, we can use simple linear interpolation to obtain acceptable results. Also, in this manner, we could generate arbitrarily dense values for $\hat{f}(r, \theta)$. This is a favorable characteristic in multimedia applications, as rough scanning is much faster than dense scanning but can still yield the dense range images most users want.

After completing the above processing, some normalization is needed to recover the original value of $f(x, y)$. If we want to recover only the matching relation between the starting positions and the ending positions, the normalization steps can be omitted, as the relative strength between $f(x, y)$ is sufficient for our purpose.

4.4. Noise and shadow handling

Another major problem involved is that we usually do not get perfect projection at every scan line. Along one scan line, a laser stripe may be missing due to shadows (e.g., see Fig. 2(b)) or because the line displacement exceeds the image boundary (e.g., see Fig. 2(a) around the center). In this case we simply treat that scan line as more sparsely sampled with respect to other scan lines (see Fig. 4(a)). That is, since we are performing integration on computers, we actually use one value in an integration interval to represent all point values in the interval, so when we get fewer data points we simply extend the length of the interval for each point. As we do not know which starting position should be dropped, we drop values in multiples of their average. In this way we greatly reduce the impact of the missing lines; at least the order of magnitude of the integration is preserved.

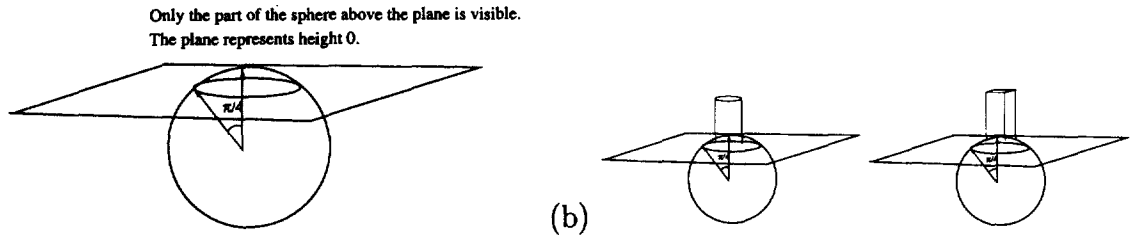

Fig. 5. The models used in the simulation. (a) The side view of the first model, representing a shadow-free 2-D circularly symmetric case. (b) Left: adding to (a) a cylinder concentric to the original sphere would produce significant shadow; however, circular symmetry is still valid. Right: by adding a square column instead of a cylinder, shadows are introduced and circular symmetry is no longer valid.

Our experiments demonstrate that our method can still recover most shapes when there is a considerable amount of missing lines.

5. Experiments and simulation

5.1. Simulations

5.1.1. Setup

To avoid introducing too many factors (e.g. noise, instrumentation faults, and so on) at the same time we create a series of simulated range images and a striping simulator to demonstrate the response of our method to individual imperfections. Missing lines and/or asymmetries are added one at a time. Fig. 5 shows the objects to be reconstructed. The simulated laser stripes are 33 parallel lines and are at exactly 45° relative to the inspection plane.

5.1.2. Results

Fig. 6 shows the original and reconstructed range image of the first model. This model is both circularly symmetric and shadow free. Fig. 7 shows the effects of shadows and the effects of both shadow and asymmetry on our reconstruction algorithm. Fig. 8 shows the laser stripe patterns for each of the two models at different angles. It is clear from the results that the output degrades as shadow increases.

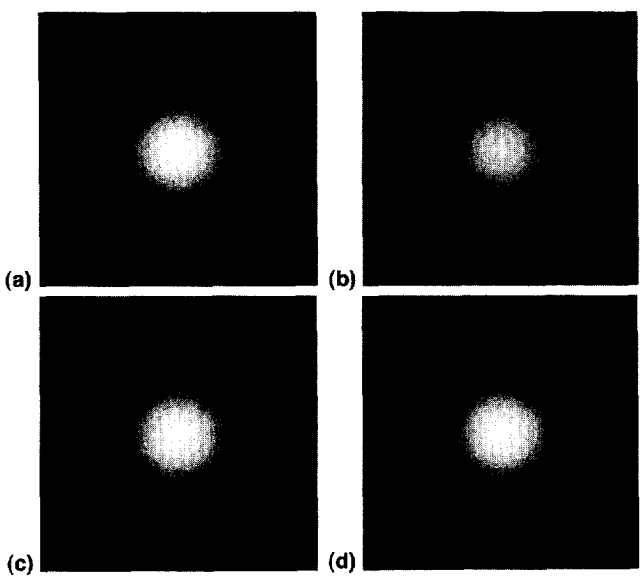

Fig. 6. Gamma-corrected range images. (a) Original partial sphere model. (b) Reconstructed image of (a) using 128 projection angles (rms = 0.23). (c) Reconstructed image of (a) using only one projection (rms = 0.16); here the circular symmetry characteristic is exploited. Note: due to digitization losses, the rotation process adds more noise, increasing rms from 0.16 to 0.23 rather than decreasing it. Furthermore, only one-half of the points are used to calculate the projection, but using our normalization method the result is almost identical to that of (d). (d) As in (c), we use only one projection, but this time all available points are used to calculate the projection (rms = 0.16).

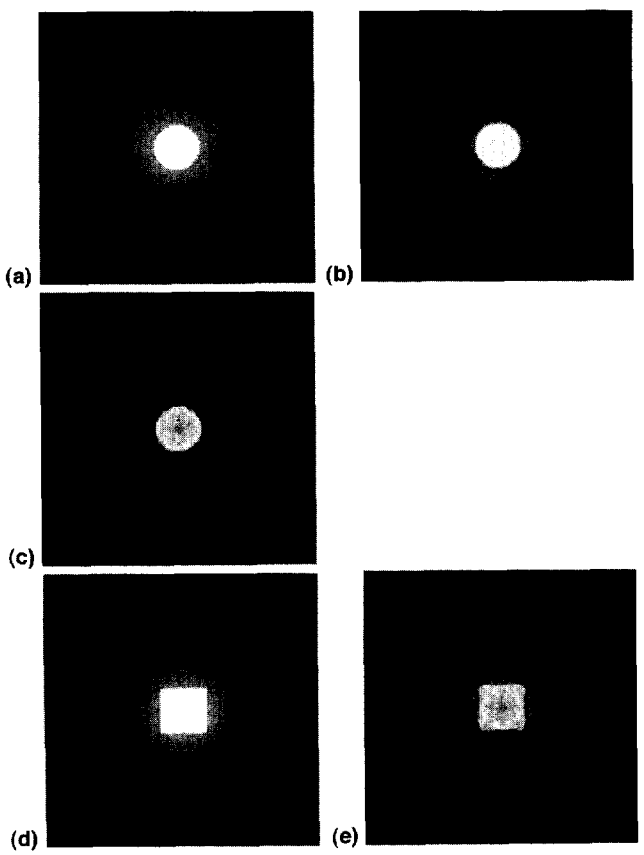

Fig. 7. Gamma-corrected range images. (a) Original range image of the model with one cylinder above the sphere. (b) Reconstructed range image using only one projection (rms = 0.64). (c) Reconstructed image using 128 projections (rms = 1.15). (d) Original range image of the model with one square pillar above the sphere. (e) Reconstructed range image using 128 projections (rms = 1.87) (rms: root mean square error).

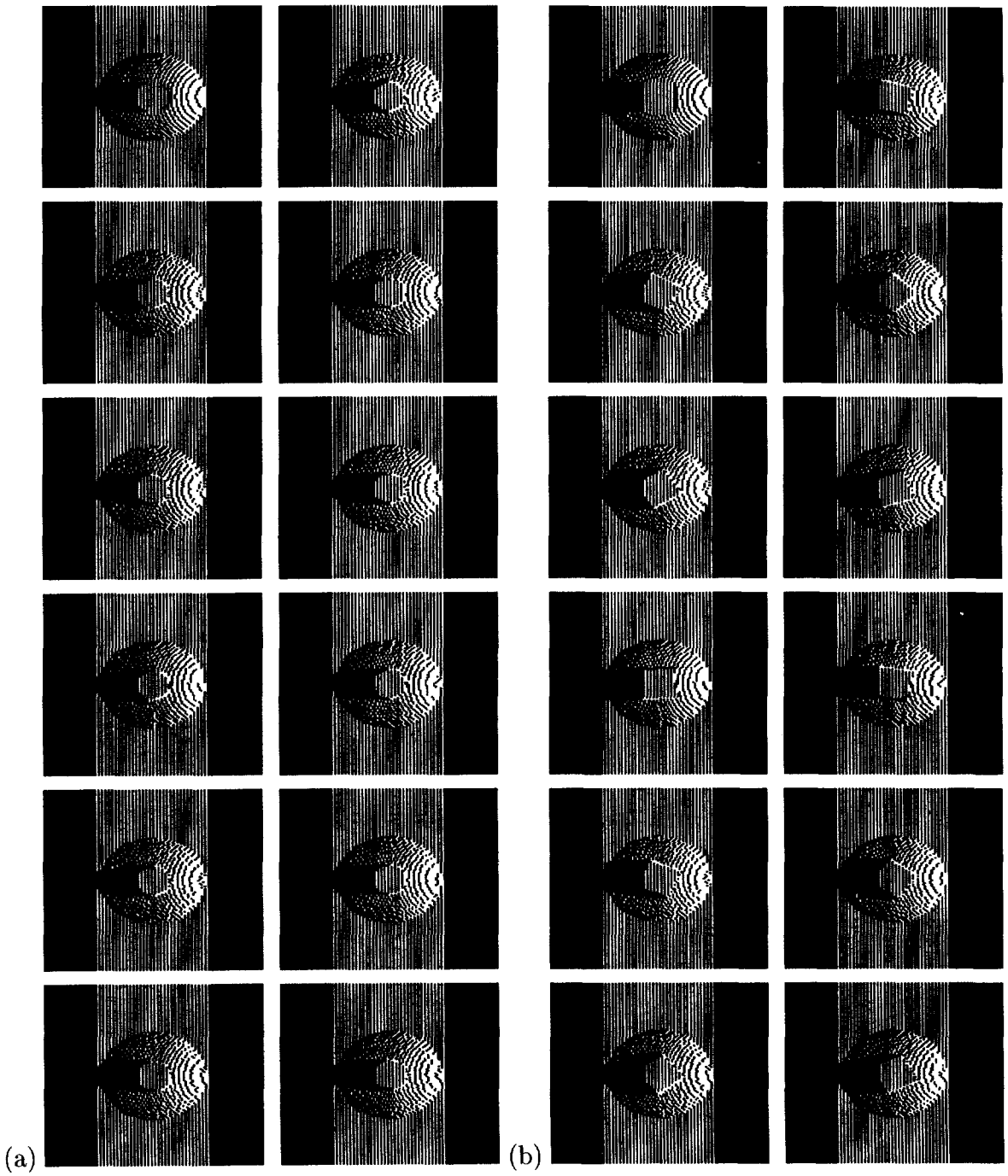

Fig. 8. Laser stripe patterns on two models with several perspectives. The simulated laser parameters are 33 parallel lines intersecting at 45° with respect to the base plane. (a) Circularly symmetric object with shadows and missing lines. Top to bottom and left to right: $\phi = 0$, $10/128\pi$, $20/128\pi$, ..., $110/128\pi$. (b) Object that is not circularly symmetric and possesses both shadows and missing lines. Top to bottom and left to right: same angles of perspective as in (a).

5.2. Experiments

5.2.1. Setup

The lenses we use include Micro-Nikkor 200 mm f/4, 55 mm f/2.8 and Kiron 105 mm f/2.8. The laser light source is Lasiris model ULF-533L which can produce 33 parallel lines simultaneously. In fact, the laser source uses lenses to diverge one single laser beam, and projects more than 33 visible light stripes simultaneously. However, only the central 33 lines are designed to be parallel. In our experience, only the central area within the 33 lines is close to being parallel under our high precision lenses.

The CCD camera employed is SONY model XC-77. It is connected to a Matrox Comet Frame Grabber on our Acer Pentium 90 PC. Our experimental set-up is illustrated in Fig. 9.

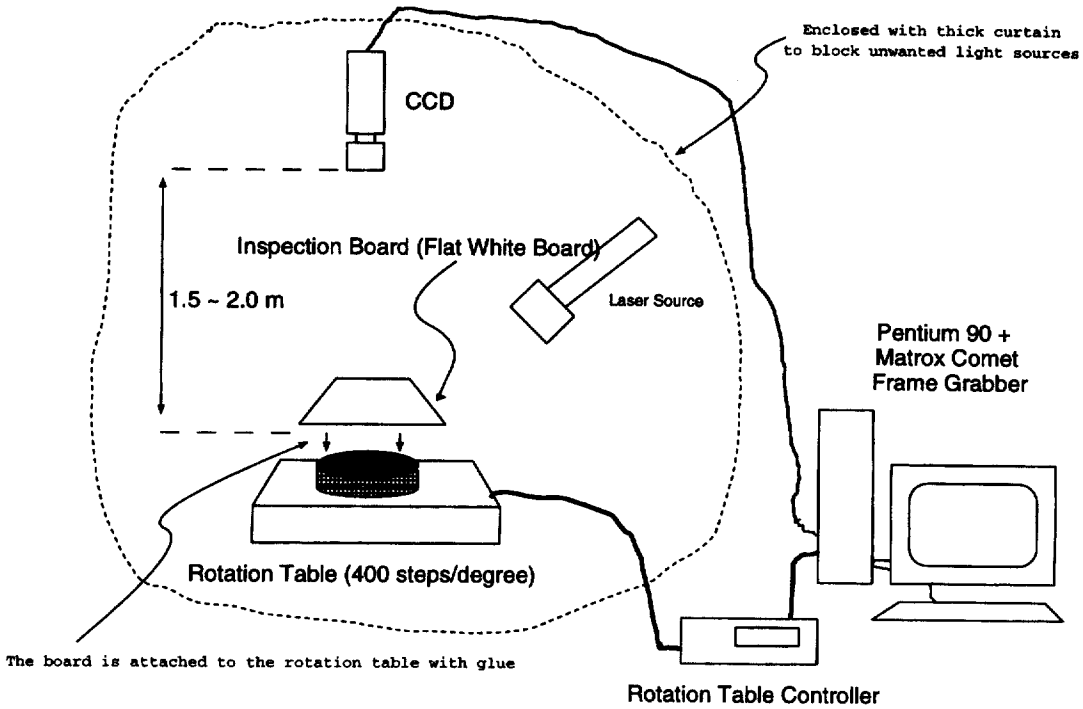

Fig. 9. The system employed to take experimental data.

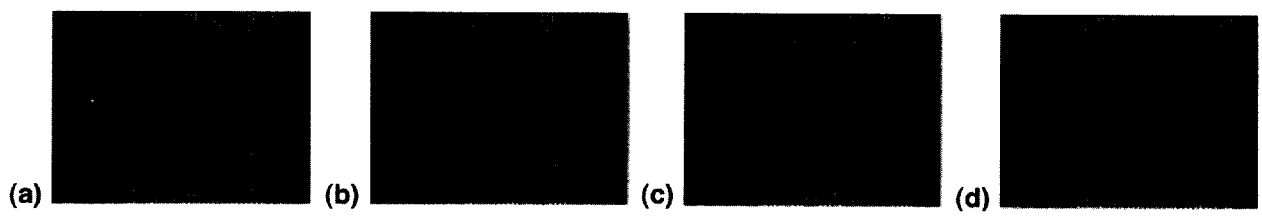

Fig. 10. Laser striping images of a padding ring, 90 views, 234 projections per view: (a) $\phi = 0$; (b) $\phi = 22/90\pi$; (c) $\phi = 44/90\pi$; (d) $\phi = 66/90\pi$.

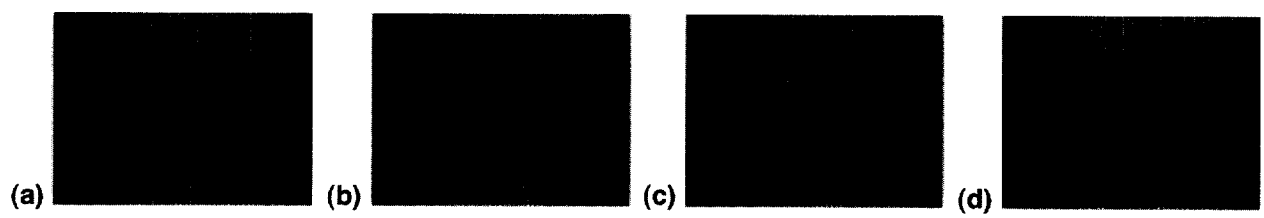

Fig. 11. Other views of the object in Fig. 10: (a) $\phi = 88/90\pi$; (b) $\phi = 110/90\pi$; (c) $\phi = 132/90\pi$; (d) $\phi = 154/90\pi$.

5.2.2. Results

We use a Sun SPARCstation 20 for reconstruction computation that takes about 8 s when we reconstruct 128 projections and 128 angles, and 3600 s for 1024 projections and 1440 angles. The complexity of our reconstruction algorithm is linear with respect to the number of angles. The number of output points in our implementation is proportional to the square of the number of projections per angle. When reconstructing Fig. 4(b) from Fig. 2(b) the single projection extracted from the real image can serve as each of the 128 projections, thanks to the circular symmetry property of this object. The extraction of laser stripe pixels can be done by smoothing followed by thresholding. The

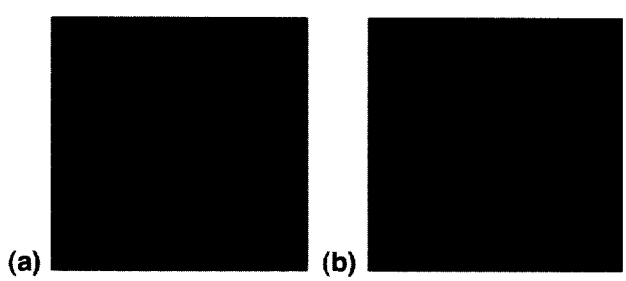

Fig. 12. (a) Reconstructed range image of one ring. (b) Double reconstruction of (a).

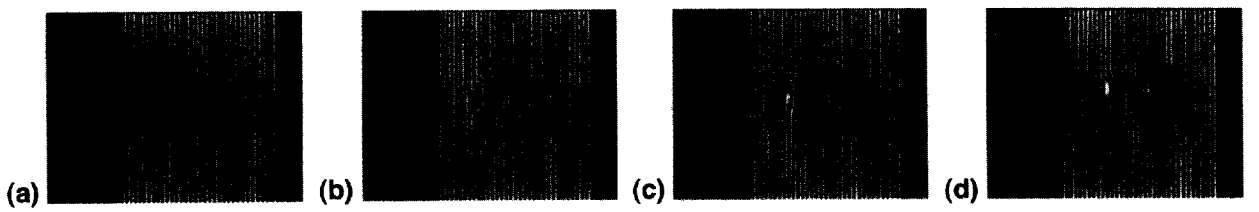

Fig. 13. Laser striping images of a stack of three padding rings, 90 views, 234 projections per view: (a) $\phi = 0$; (b) $\phi = 22/90\pi$; (c) $\phi = 44/90\pi$; (d) $\phi = 66/90\pi$.

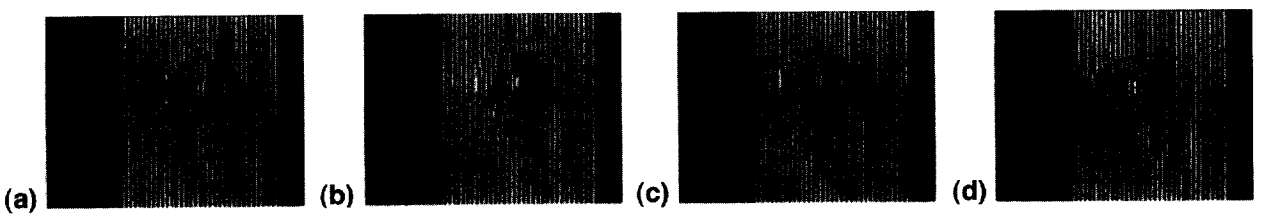

Fig. 14. Other views of the object in Fig. 13: (a) $\phi = 88/90\pi$; (b) $\phi = 110/90\pi$; (c) $\phi = 132/90\pi$; (d) $\phi = 154/90\pi$.

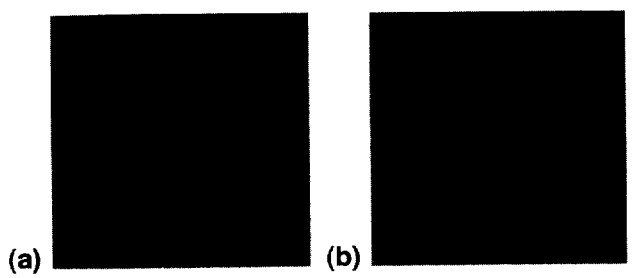

Fig. 15. (a) Reconstructed range image of three metal rings in a pile. (b) Double reconstruction of (a). The ring area, demarcated manually, has an average value 2.9 times that of Fig. 12.

centroid of a cluster of stripe pixels can be treated as the position of a laser stripe.

Fig. 10 shows one metal ring placed on the inspection board. Fig. 12(a) is the reconstruction result of Fig. 10 and Fig. 11. In Fig. 12(b) 'double reconstruction' means that we actually rotate the object 360°. Though the projection from 0° to 180° is identical with that of 181° to 360° in a continuous domain, i.e. an infinitely dense laser stripe distribution, it may not be the case in our sparsely distributed laser stripe system, especially when the object being inspected has a complex, asymmetric shape and is not positioned at the rotation center. So, 'double reconstruction' incorporates more viewing angles than 'single reconstruction'.

Figs. 13–15 are similar to the previous set, except that this time we stack up three metal rings so we can see them display a longer shadow than in the one-ring case.

The above two cases can also be used to find the rotation center. Simply calculate the laser stripe displacement centroid in every view angle and then take the average of them; we then get the row position of the rotation center.

The model plane pictures (Figs. 16–27) are taken to illustrate the performance of our system on complex surfaces. All model planes are light peach in color except the A-7 Corsair attack jet, which is dark red. The range images use darker color to represent closer distance from our camera. We pick eight different views of raw pictures in each case, and the divisor number in its caption indicates how many angles are used in that set. We can see clearly that by increasing the number of view angles we can significantly improve the quality of the results.

Since the model planes we use are made of elastic rubber, we do not have any other non-contact measurement instrument to verify our results in these cases. One can estimate the errors using the errors of a flat plate, though. As a rule of thumb, in a smooth, shadowless area one can expect the error rate to be close to that of a flat plate. In a complex, shadow-haunted area one can add 1 mm to 2 cm to the corresponding flat plate error rate (see Table 1).

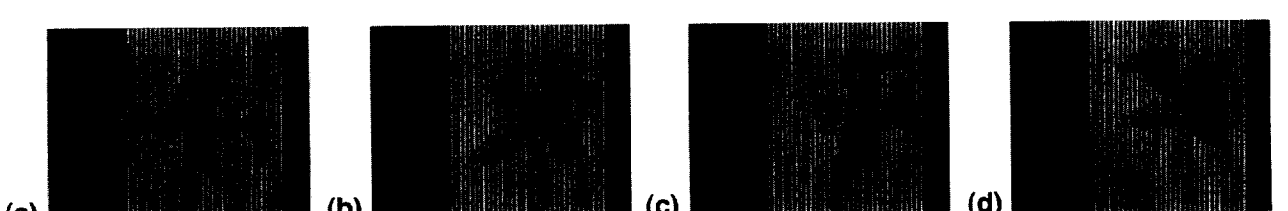

Fig. 16. Laser striping images of a light peach model plane (an EA-6 Prowler Jammer), 90 views, 234 projections per view: (a) $\phi = 0$; (b) $\phi = 22/90\pi$; (c) $\phi = 44/90\pi$; (d) $\phi = 66/90\pi$.

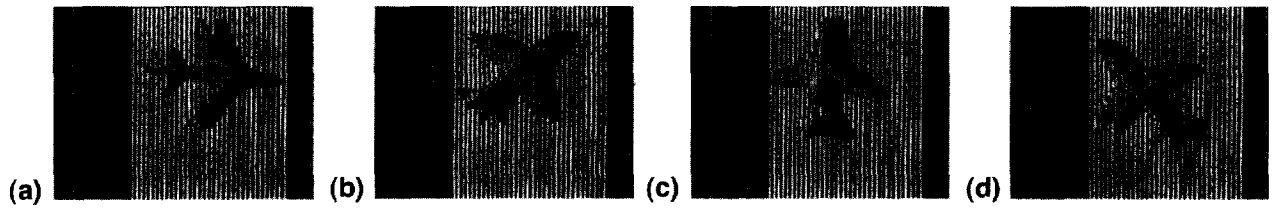

Fig. 17. Other views of the object in Fig. 16: (a) $\phi = 88/90\pi$; (b) $\phi = 110/90\pi$; (c) $\phi = 132/90\pi$; (d) $\phi = 154/90\pi$.

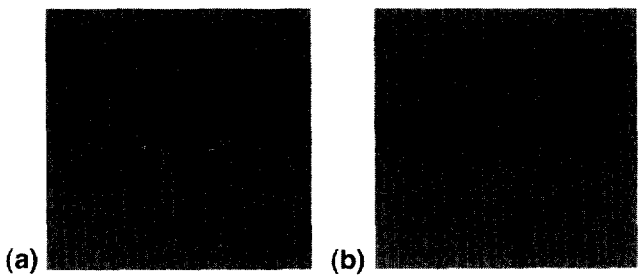

Fig. 18. (a) Reconstructed range image of previous model plane. (b) Double reconstruction of (a).

6. Comparisons and discussions

6.1. Comparison

As mentioned previously, Jarvis [7] surveyed several range finding techniques. Within the scope of multistriping laser systems, the shuttering solution [4] is generally faster, but one needs a good shutter for the algorithm to work. The proposed new approach is faster when inspecting more symmetric objects, and needs no shutter support.

The best case for our method is circularly symmetrical objects, in which case only one picture is enough to resolve any ambiguity. In this case the complexity relative to the number of stripes used is constant. Not everything is circularly symmetric, but circular symmetry is a property often possessed among manufactured objects, and these mass-produced parts mostly require machine vision inspection. Other good examples are the rotor, the propeller, and the turbine fan. If there are four blades on the rotor or propeller, then we need only one fourth the number of pictures needed for general objects to resolve ambiguity. From the steam power plant to the jet engine, turbine fans are widely used today, and their frontal view is very close to circular symmetry.

Another feature of the proposed method is its ability to generate dense range images. The optical shuttering solution uses $\log N$ pictures to resolve the ambiguity arising from using 'one' picture. All $\log N$ pictures are taken at exactly the same relative position between the inspection system and the object. This is rather wasteful if what we want is the complete surface shape of an object. For general objects our method needs many more pictures than $\log N$, but each picture used views the object from a different angle. When our algorithm finishes processing, all ambiguity in each multistripe picture is solved simultaneously, and we get significantly more range data points than when we use the optical shuttering solution. In effect, our method batches all the ambiguity resolution work together and collects more

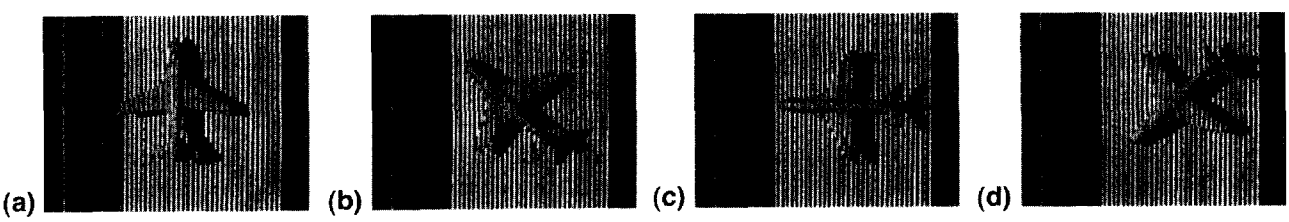

Fig. 19. Laser striping images of a light peach model plane (an EA-6 Prowler Jammer), 180 views, 234 projections per view: (a) $\phi = 0$; (b) $\phi = 45/180\pi$; (c) $\phi = 90/180\pi$; (d) $\phi = 135/180\pi$.

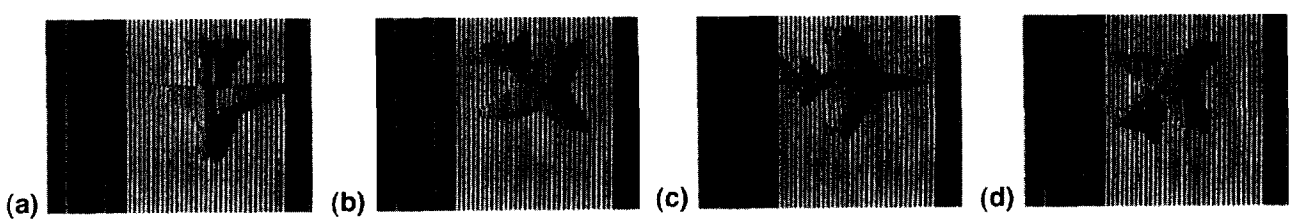

Fig. 20. Other views of the object in Fig. 16: (a) $\phi = 180/180\pi$; (b) $\phi = 225/180\pi$; (c) $\phi = 270/180\pi$; (d) $\phi = 315/180\pi$.

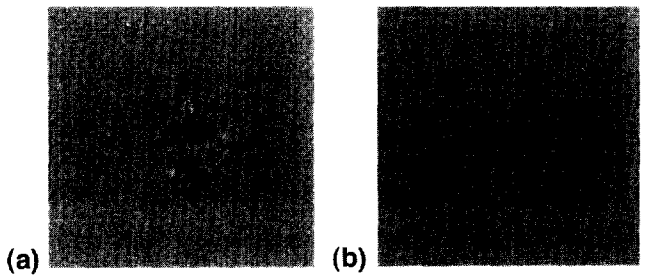

Fig. 21. (a) Reconstructed range image of previous model plane. (b) Double reconstruction of (a).

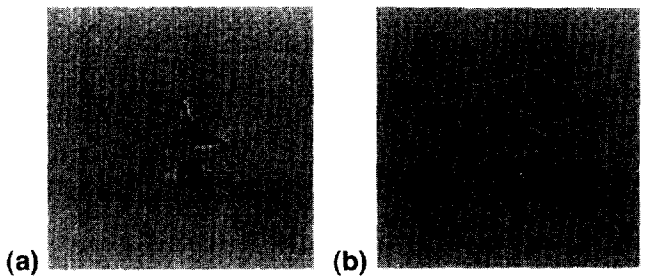

Fig. 24. (a) Reconstructed range image of previous model plane. (b) Double reconstruction of (a).

range data per picture taken. The optical shuttering method is more accurate for each range datum taken, but collects fewer range data per picture taken.

6.2. Discussion

Due to noises and shadows, the projection data acquired at different angles may need to be checked by cross-validation. If certain projections fail to pass the check, we can drop these projections and use the incomplete angular range reconstruction method devised in [10].

Increasing the stripe density is not so easy as most people might think. Splitting one laser source into more lines makes the intensity of each line weaker. The weaker the line, the more difficult it is to separate a laser stripe from noise. For example, Fig. 2(a) can be taken by turning off only part of the lights in our laboratory, while Fig. 2(b) must be taken in a totally dark room in order for the stripes to have the same relative intensity as in Fig. 2(a).

Ignoring the effects of camera resolution, the higher stripe density means a higher sampling rate, and reveals finer details for the objects being investigated. However, higher stripe density means thinner stripe width if the camera resolution remains unchanged. Stripes with widths only a few pixels wide become missing easily, either during the digitization of our CCDs or during the stripe recognition phase, thus introducing more errors into our data sets. In our experiments, we set up our image acquisition system for optimal image quality of our laser stripes.

Another problem of increasing the number of laser stripes using lenses is that the curvature of each line increases as it is farther from the original center. This is the result of light diffraction and interference, and this phenomenon becomes more prominent as the density of stripes increases.

The resolution of the CCD camera is another bottleneck. High resolution CCDs are prohibitively expensive, and, even if we can afford it, the maximum resolution of silicon-based CCD technology is limited by the laws of quantum physics.

In view of this, our rotation reconstruction method can be deemed as a last resort to increase the density of the output range data. When we can stuff no further recognizable laser stripes into a single angle, we simply rotate and reconstruct several angles using the method we have proposed. By comparing the image of one view and the final reconstruction result, one can see the great increase in resolution.

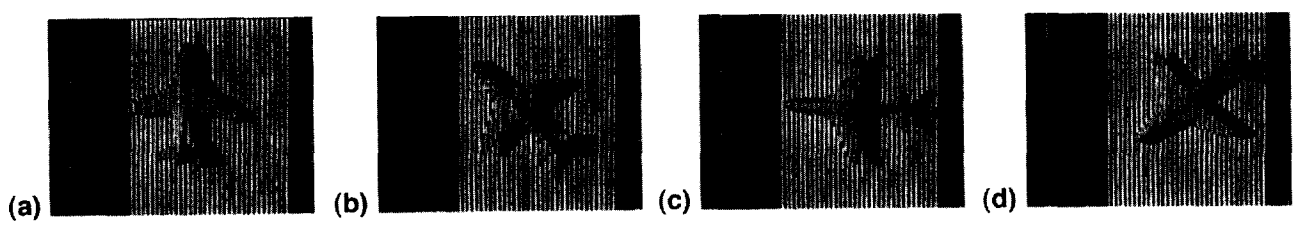

Fig. 22. Laser striping images of a light peach model plane (an EA-6 Prowler Jammer), 720 views, 234 projections per view: (a) $\phi = 0$; (b) $\phi = 180/720\pi$; (c) $\phi = 360/720\pi$; (d) $\phi = 540/720\pi$.

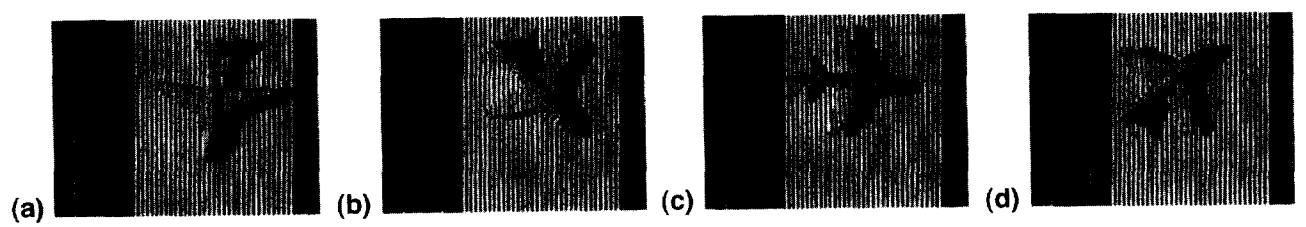

Fig. 23. Other views of the object in Fig. 16: (a) $\phi = 720/720\pi$; (b) $\phi 900/720\pi$; (c) $\phi = 1080/720\pi$; (d) $\phi = 1260/720\pi$.

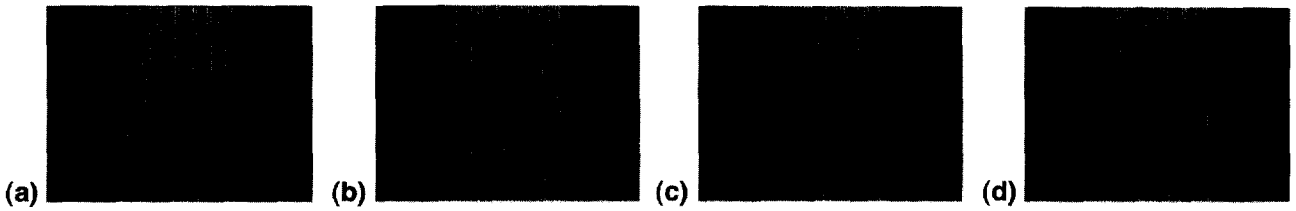

Fig. 25. Laser striping images of a dark red model plane (an A-7 Corsair Attack Jet), 40 views, 234 projections per view: (a) $\phi = 0$; (b) $\phi = 10/80\pi$; (c) $\phi = 20/80\pi$; (d) $\phi = 30/80\pi$.

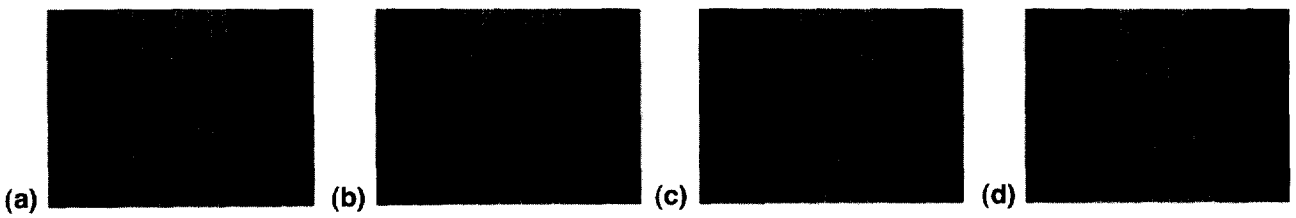

Fig. 26. Other views of the object in Fig. 25: (a) $\phi = 40/80\pi$; (b) $\phi = 50/80\pi$; (c) $\phi = 60/80\pi$; (d) $\phi = 70/80\pi$.

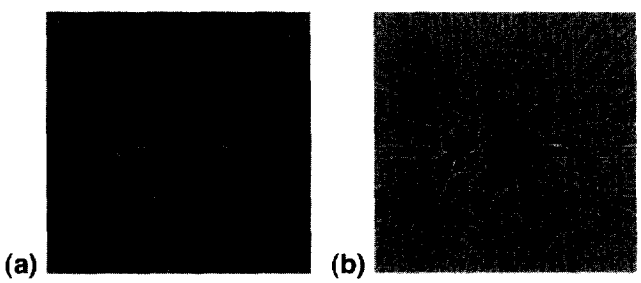

Fig. 27. (a) Reconstructed range image of previous model plane. (b) Double reconstruction of (a).

7. Conclusion and future work

7.1. Conclusion

When a complete profile of a side of an object is needed, the proposed resolution is better than most existing ones. Furthermore, when circular symmetry is present, our method requires the fewest number of pictures — one. In terms of precision, this method could be used to increase the density of range data output when the stripe density of one view cannot be increased because of physical limitations.

7.2. Future work

We will try to eliminate some artifact problems inherent in the Fourier slice theorem. Also, we are still working on improving the stripe recognition algorithms and seeking ways to increase the line density of each view.

Table 1
Flat plate error chart

No. of lines	No. of angles	No. of projections	Flat plate error
33	40	234	1.5 mm
33	90	234	0.5 mm
33	180	234	0.4 mm
33	720	234	0.15 mm

Acknowledgements

This research was supported by National Science Council of Taiwan, ROC, under Grants NSC 85-2212-E-002-077 and NSC 86-2212-E-002-025, by Mechanical Industry Research Laboratories, Industrial Technology Research Institute under Grant MIRL 863K67BN2, by EeRise Corporation, ACME Systems, Mosel Vitelic and Foxconn Inc.

References

[1] S.S. Lin and C.S. Fuh, Range data reconstruction using Fourier slice theorem, Proceedings of the 13th International Conference on Pattern Recognition, Vienna, Austria, 1996, pp. 874–878. IEEE Computer Society Press.
[2] P.M. Will, K.S. Pennington, Grid coding: A novel technique for image processing, Proceedings of the IEEE 60 (1972) 669–680.
[3] J.A. Jalkio, R.C. Kim, S.K. Case, Three dimensional inspection using multistripe structured light, Optical Engineering 24 (1985) 966–974.
[4] R. Jain, R. Kasturi and B.G. Schunck, Machine Vision, McGraw-Hill, New York, 1995, pp. 300–304.
[5] K.L. Boyer, A.C. Kak, Color-encoded structured light for rapid active ranging, IEEE Transactions on Pattern Analysis and Machine Intelligence 9 (1987) 14–28.
[6] F.W. DePiero and R.L. Kress, Design of a structured light sensor for in situ calibration, Proceedings of the 1995 IEEE/RSJ International Conference on Intelligent Robots and Systems, Pittsburgh, PA, 1995, pp. 513–518.
[7] R.A. Jarvis, A perspective on range finding techniques for computer vision, IEEE Transactions on Pattern Analysis and Machine Intelligence 5 (1983) 122–139.
[8] V. Sequeira, J.G.M. Goncalves, M.I. Ribeiro, 3D environmental modelling using laser range sensing, Robotics and Autonomous Systems 16 (1995) 81–91.
[9] Z.H. Cho, J.P. Jones and M. Singh, Foundations of Medical Imaging, Wiley, New York, 1993.
[10] S.E. Sysoev, Reconstruction of a function of two variables from the

data of its exponential radial transform in the case of an incomplete angular range, Communications of the Moscow Mathematical Society 49 (1994) 180–181.

[11] W.H. Press, B.P. Flannery, S.A. Teukolsky and W.T. Vetterling, Numerical Recipes in C, Cambridge University Press, Cambridge, UK, 1988, pp. 398–414.